

# Plasma Electrolytic Oxidation of Nanocomposite Coatings on Ti-6Al-7Nb alloy for Biomedical Applications

Qabas Khalid Naji\*, Jassim Mohammed Salman, Nawal Mohammed Dawood

Department of Metallurgical Engineering, College of Materials Engineering, University of Babylon, Babylon, Iraq.

\*Corresponding Author.

Received 18/10/2023, Revised 28/10/2023, Accepted 30/10/2023, Published Online First 20/04/2024,  
Published 01/11/2024



© 2022 The Author(s). Published by College of Science for Women, University of Baghdad.

This is an open-access article distributed under the terms of the [Creative Commons Attribution 4.0 International License](https://creativecommons.org/licenses/by/4.0/), which permits unrestricted use, distribution, and reproduction in any medium, provided the original work is properly cited.

## Abstract

The current study aims to use Ti-6Al-7Nb alloy instead of Ti-6Al-4V alloy in medical applications. Due to the poor hardness and wear that cause loose of the implant. The surface of Ti-6Al-7Nb alloy has been coated with titanium and zirconia/titanium oxide nanocomposite coating by Plasma electrolytic oxidation (PEO) process. The results of the tests showed the possibility of deposition of ceramics coatings on the surface of Ti-6Al-7Nb alloy by using different times. The ceramics layer of titanium oxide (TiO<sub>2</sub>) is formed during coating porous, homogenous distribution, and low corrosion rate and wettability. A composite nano ceramic layer was obtained from nano ZrO<sub>2</sub> with TiO<sub>2</sub> observed with increased thickness layer and concentration with time compared TiO<sub>2</sub> layer improved percentage (90.5%) during the corrosion test, Hank's solution showed a strong ability to act as a barrier to prevent the localized corrosion attack from many aggressive ions.

**Keywords:** Corrosion Resistances, Medical Applications, Plasma electrolytic oxidation (PEO), Porosity, Titanium oxide (TiO<sub>2</sub>).

## Introduction

Orthopedic implant failure is mostly brought on by wear, which is also proven to hasten corrosion. As a result, orthopedic implants are usually made from high wear-resistant materials such as ceramics and Co-Cr<sup>1</sup>. The ball of hip implants is constructed of Co-Cr or other strong ceramics, while the femoral component is exclusively comprised of Ti-based alloys<sup>2</sup>. The type and amount of corrosion products that these orthopedic implants release into the body, on the other hand, continues to be a major concern<sup>3</sup>. As a result, metallic biomaterials' corrosion resistance is critical. Titanium and its alloys, unlike many other materials, corrode either rapidly or slowly, depending on the environment<sup>4</sup>. Titanium and titanium-based alloys are utilized extensively in biomedical and dental applications, as previously

stated. This is due in part to the native titanium dioxide layer that shields the metal from further oxidation<sup>5</sup>. The major consideration when designing and selecting metals and alloys for in vivo use is corrosion. During corrosion processes, allergenic, toxic/cytotoxic, or carcinogenic species (e.g., Ni, Co, Cr, V, Al) may be released into the body<sup>6</sup>. Metals may be regarded as the most important technical materials, and because of their excellent mechanical properties and great heat conductivity, they are used as biomaterials<sup>7</sup>. It is essential for a metal to be biocompatible, or not cause an undesirable reaction, when used as a biomaterial<sup>8</sup>. For load-bearing implants and inner fixing systems, metallic materials are the most frequently used. The primary functions of orthopedic implants systems are to restore the

load-bearing joints function that undergoes elevated levels of mechanical stress, wear, and fatigue during ordinary activity<sup>9</sup>. Important orthopedic implants are prostheses for ankle, knee, hip, shoulder, and need equipment like cables, screws, plates, pins, etc. that used in the fixation of fracture<sup>10</sup>. Metals are powerful, and most of them are capable to be formed into complicated forms. During or after final formation, the required mechanical characteristics of metals can be accomplished by heat and mechanical processing. In addition, the correct treatment of components produced from chosen metal compositions can achieve a degree of corrosion and wear resistance. The high tensile strength, high yield strength, fatigue resistance, and corrosion resistance is some of the features of metallic materials<sup>11</sup>. The oxide layer of the Ti-alloys surface, which is generally a few nanometers thick, has high passivity and resistance to chemical attack<sup>12</sup>. Due to the coarse microstructure of cast alloys (as shown by a high coefficient of friction), weak shear strength, low fatigue strength, and constrained elongation compared to wrought alloys, titanium, its alloys have a high price as well as a significant sensitivity to friction and wear. Therefore, further microstructural modification is typically required to improve mechanical qualities while maintaining the product's form<sup>13</sup>. Biomedical implants frequently have their surfaces altered to increase biocompatibility, surface roughness, corrosion resistance, and wear resistance<sup>14</sup>. In addition to enhancing other desirable features, all revised surfaces should be examined for corrosion behavior. In order to create implants that can withstand in the human system for a longer period of time. A thorough understanding of the interactions that take place at the atomic level between the surface of the implant, the host, and the biological environment, including all types of micromotions of the implants kept inside the human

system, should be studied in more detail to develop implants that can withstand in the human system for a longer period of time<sup>15</sup>. The material surface plays an extremely important role in the response of the environment to artificial medical devices<sup>16</sup>. Surface modification improves adhesion qualities, micro cleaning, functionalization of amine, and biocompatibility in addition to changing the surface's look<sup>17</sup>. In order to manage the appropriate biological response in a particular cell/tissue situation, various surfaces may be generated utilizing the surface modification technique, with the aim of speeding up healing and preventing adverse effects<sup>18</sup>. Because titanium and its alloys have poor tribological properties, such as low wear resistance, the implant's service life is shortened. Surface coatings can help to solve this problem to a considerable extent. Titanium orthopedic devices can function much better thanks to surface engineering, beyond their intrinsic capacities<sup>19</sup>. Plasma allowing categories broadly describe all conceivable surface changes<sup>20,21</sup>. Plasma electrolytic oxidation (PEO) is an electrochemical surface treatment process to produce oxide protective coatings on some metals. PEO can be regarded as a developed method from anodic oxidation by discharging sparks at a high voltage which is also named anodic spark oxidation or Micro-Arc oxidation<sup>22</sup>. Many research utilized synthetic nanoparticles like ZrO<sub>2</sub>, the results showed enhancement for some tested mechanical properties. Also, using a of ZrO<sub>2</sub>/TiO<sub>2</sub> introduced higher property values<sup>23</sup>.

In this study, TiO<sub>2</sub>, and ZrO<sub>2</sub>/TiO<sub>2</sub> nanocomposite coatings on Ti-6Al-7Nb alloy by Plasma electrolytic oxidation (PEO) were researched using various experimental instruments to improve biocompatibility, and corrosion resistance of implants.

## Materials

Standard structural titanium alloy (Ti-6Al-7Nb) discs with the following dimensions (13mm3mm, 99.9% pureness) have been created by cutting the rod

in a water-cooled cutter wheel. Table 1 shows the (Ti6Al7Nb) alloy's chemical composition<sup>7</sup>. To clean the specimens, water-resistant SiC abrasive paper up to #800 was used<sup>24</sup>.

**Table 1. Chemical Analysis of Ti6Al7Nb alloy <sup>7</sup>.**

Element	Al	Nb	Fe	Ta	O	C	N	H	Ti
ASTM(Wt%)	5.5-6.5	6.5-7.5	≤ 0.25	≤ 0.50	≤ 0.20	≤ 0.08	≤ 0.05	≤ 0.009	Rem.
Wt%	6.15	7.28	0.20	0.46	0.17	0.078	0.043	0.0087	Rem.

## Methods

The specimen has been used as polished stainless 316L plate and positive electrodes (anodes). Has served as the cathode. The ceramic coatings were deposited using a Dc-Ac home-made PEO method, which controlled the voltage in galvanostatic mode. Using a magnetic stirrer for two hours to produce the electrolyte solution, it was then sonicated in an ultrasonic bath. Compounds used in electrolyte solutions and process variables are listed in Table 2. Show that sample (A) coated with TiO<sub>2</sub>/Ti-6Al-7Nb alloy and sample (B) coated with ZrO<sub>2</sub>/TiO<sub>2</sub>/Ti-6Al-7Nb alloys with different duration. During cleanup, the temperature might be kept at or below 40 degrees centigrade. After the first oxidation, the samples were cleaned with fresh distilled water.

**Table 2. Electrolytes Composition utilized for PEO Processing.**

Code of specimens	Electrolytes Composition <sup>21</sup>	Voltages	Duration
A1	Na <sub>2</sub> CO <sub>3</sub> =10g/l Na <sub>2</sub> SiO <sub>3</sub> =2g/l	400	5min
A2	Na <sub>2</sub> CO <sub>3</sub> =10g/l Na <sub>2</sub> SiO <sub>3</sub> =2g/l	400	10min
B1	ZrO <sub>2</sub> =3g/l, Na <sub>3</sub> PO <sub>4</sub> =5g/l, KOH=1g/l	400	5min
B2	ZrO <sub>2</sub> =3g/l, Na <sub>3</sub> PO <sub>4</sub> =5g/ KOH=1g/l	400	10min

To estimate phasing compositions, X-ray diffraction studies were conducted using a DX-2700 X-Ray Diffractometer with Cu K radiation ( $\lambda = 1.5405$ ) and a scanning speed of 5/min from 10° to 80° of 2. The topography and microstructure of the blanks and films have been studied using scanning electron microscopy (SEM) type (FEI, Quanta 450, Czech) and EDS analysis. The contacting angles of the test specimen surface were measured using a contacting angle metre (DSA100, KRÜSS, Germany). After 1 minute, a 2L droplet of ringer solution was put onto the specimen surface, and the contacting angle was determined. Hank's solution (the chemical composition of which is shown in Table 3) for this research had a pH of 7.4 at 37°C±1 degrees centigrade. The value of corrosion rate can be determined from the data of this test according to [ASTM G102] as follows in Eq. 1<sup>25</sup>.

**Table 3. Hank's solution's Chemical Structure <sup>19</sup>.**

Substance (g/l)	NaCl	CaCl <sub>2</sub>	KCl	NaHCO <sub>3</sub>	Glucose	MgCl <sub>2</sub> .6H <sub>2</sub> O	Na <sub>2</sub> HPO <sub>4</sub> .2H <sub>2</sub> O	KH <sub>2</sub> PO <sub>4</sub>	MgSO <sub>4</sub> .7H <sub>2</sub> O
Amount	8	0.14	0.4	0.35	1.0	0.1	0.06	0.06	0.06

$$\text{Corrosion rate} = K \times i_{corr.} \times \frac{EW}{D} \quad 1$$

Where:

[Corrosion rate = (mm/year), K = 3.27×10<sup>-3</sup> mm g/μA cm year, D= material density (g/cm<sup>3</sup>), i<sub>corr.</sub>= corrosion current density (μA/cm<sup>2</sup>), and EW= Equivalent weight] <sup>25</sup>.

## Results and Discussion

### Phase identification of PEO coatings

The XRD results proved the deposition of the titanium oxide layer after PEO on the surface of the Ti-6Al-7Nb alloy substrate at (400V&5min) in Fig. 1 (a). The formation of TiO<sub>2</sub> layer on the surface of

specimen A1 has crystalline phases: rutile (tetragonal) and anatase (tetragonal) phases also the (α-HCP) and (β-BCC) return to the Ti-alloy. While the strength of the Ti-alloy peaks dropped during the MAO process at 300V, the rutile TiO<sub>2</sub> (200), (211),

and (202) and titania crystals (anatase) (101), (103), and (200) peaks at  $2^\circ$  (39.3, 54.2, and 76.0) are both much stronger than those of the untreated Ti sample<sup>26</sup>. For medicinal applications, the rutile phase of titania is more crucial than other forms. This is because both crystal types have energy gaps, but anatase has more pores and is used in optical applications while rutile has a lower energy gap and is more stable at higher temperatures. Anatase to rutile conversion happens depending on the temperature and duration of plasma micro discharges, which is why it is used in medical applications<sup>26</sup>. The intensity of the peaks slightly increased with the increasing time, which could be related to the oxide layer growth as shown in Fig. 1 (b) at 10min. Therefore, it is anticipated that the combination of anatase and rutile crystal phases in the coated Ti-alloys specimen created in this study may favorably affect the bioactivity of Ti-alloys by boosting the osteogenic capabilities of Ti-alloys<sup>27</sup>.

In Fig. 1 (c, and d), The well-crystallized Zirconia (tetragonal) phase and (anatase, rutile) phases at  $\text{TiO}_2$  could be identified in different time periods based on the XRD patterns of  $\text{ZrO}_2/\text{TiO}_2$  nanocomposite coatings. The peaks are made of  $\text{ZrO}_2$  with anatase and rutile phases. The phases of  $\text{ZrO}_2$  at specimen B1 had modest intensities at (400V & 5min). In fact, the discharge process can quicken hydrolysis, resulting in an increase in  $\text{ZrO}_2$  and  $\text{TiO}_2$  in the channel at high temperatures and high pressures during PEO process at high time. The intensity of the zirconia peak grew steadily throughout increased time PEO process when the Ti-6Al-7Nb alloy substrates were exposed to the surface. The strength of the peaks  $2^\circ$  (27.5 & 34.1) at (002) and (111) achieved the maximum coating, which revealed a strong  $\text{ZrO}_2$  phase with a maximum thickness. We could also detect that both the intensities of the rutile and anatase peaks grew steadily.

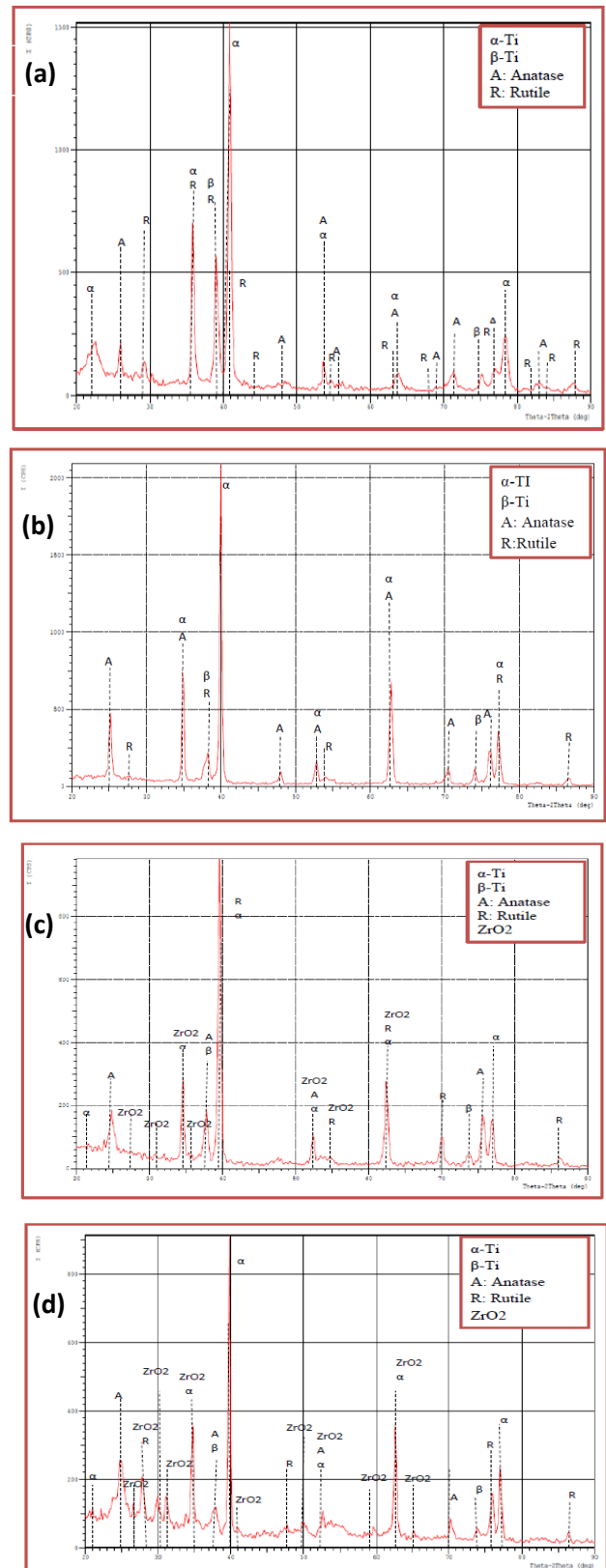


**Figure1. XRD of  $\text{TiO}_2$ , and  $\text{ZrO}_2/\text{TiO}_2$  by PEO Process with different time (a) A1 sample, (b) A2 sample, (c) B1 sample, and (d) B2 sample.**

### Surface morphology of the coating

The FESEM results of the coated specimen from Fig.2(a), which show that for the surface morphology of the oxide layer  $\text{TiO}_2$  to the Ti-6Al-7Nb alloys at different magnifications treated by PEO process was relatively rougher and exhibited a grainy structure with a limited amount of pores with different sizes by the spark discharges. The PEO coating showed two types of pores: micro-pores and sub micro-pores. The micro-pores had a roughly circular or elliptical shape like volcanic vent<sup>28</sup>. A typical porous structure was also found in coating of sample A2, whereby the pore size was clearly dependent on the limiting time as shown in Fig. 2(b). Pores with maximum diameters and homogenous distributions can be observed on the surface of the Ti- alloy. As the voltage increased, it was clearly seen that the diameter of such pores and the surface roughness increased accordingly. The pores sizes increased, and the coating surface gradually became rough. Both materials have an oxide layer made up of many micro protrusions with regularly spaced holes that range in size from sub-micron to a few microns. When compared to an uncoated polished surface, the presence of this porosity promotes the phenomenon of osseointegration because the pores operate as sites that enhance the contact area between the bone and the implant for bone tissue development, improving their anchoring in addition to the advantages connected to their ability to retain bioactive components<sup>29</sup>.

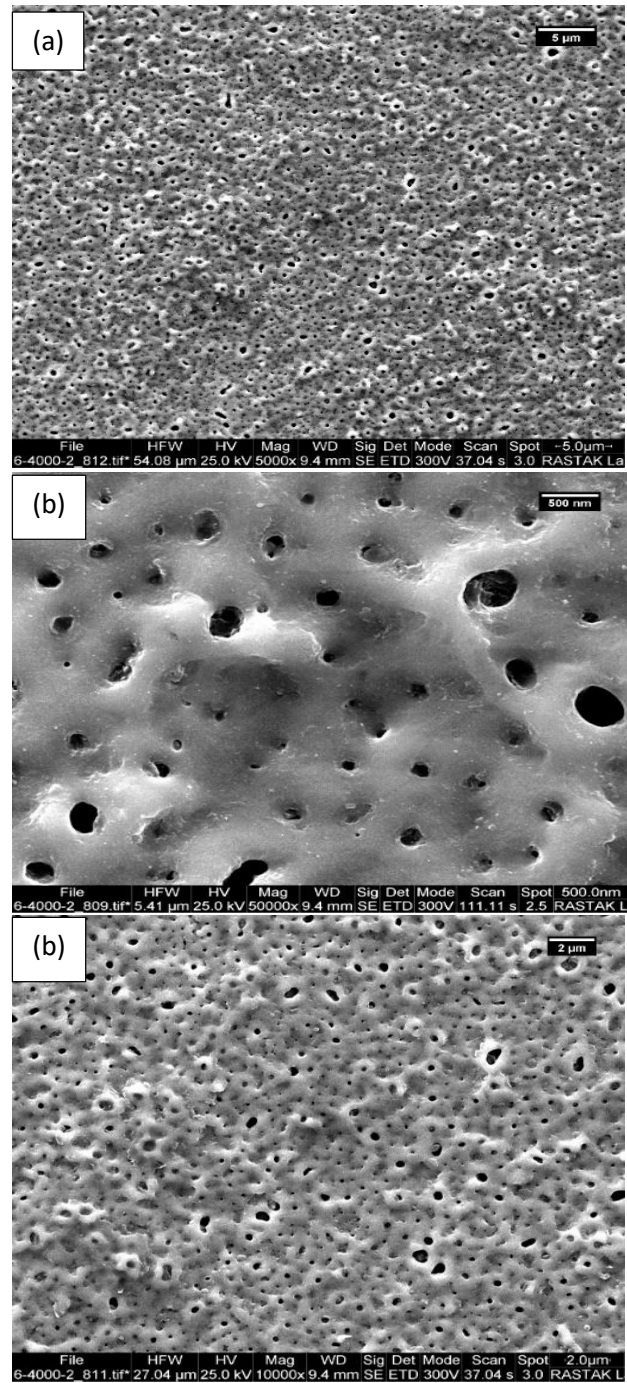
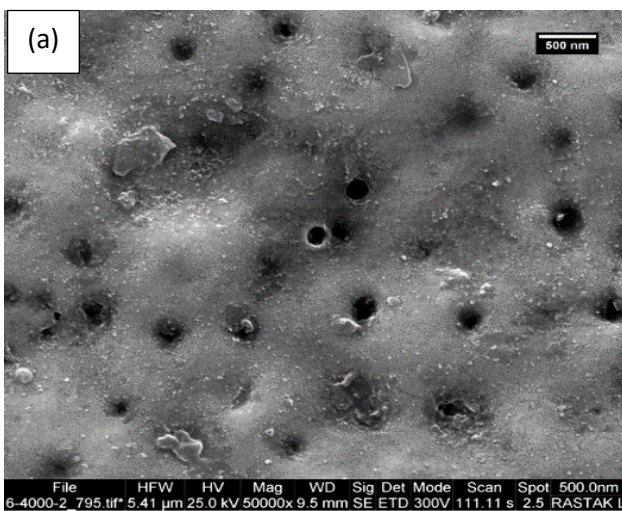
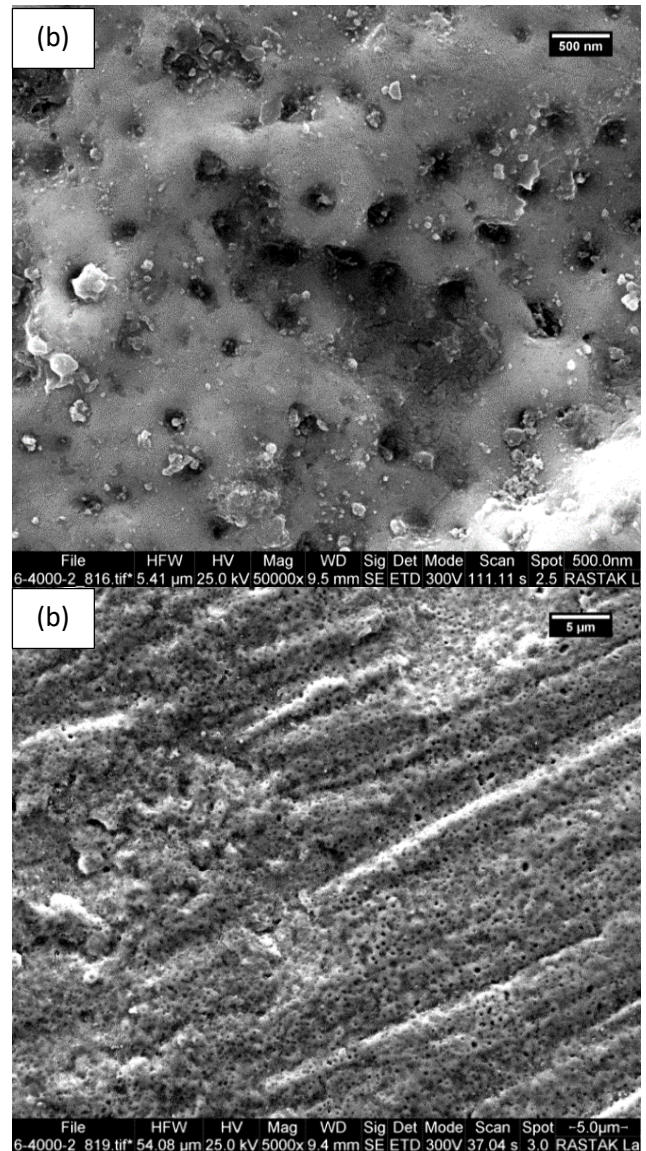
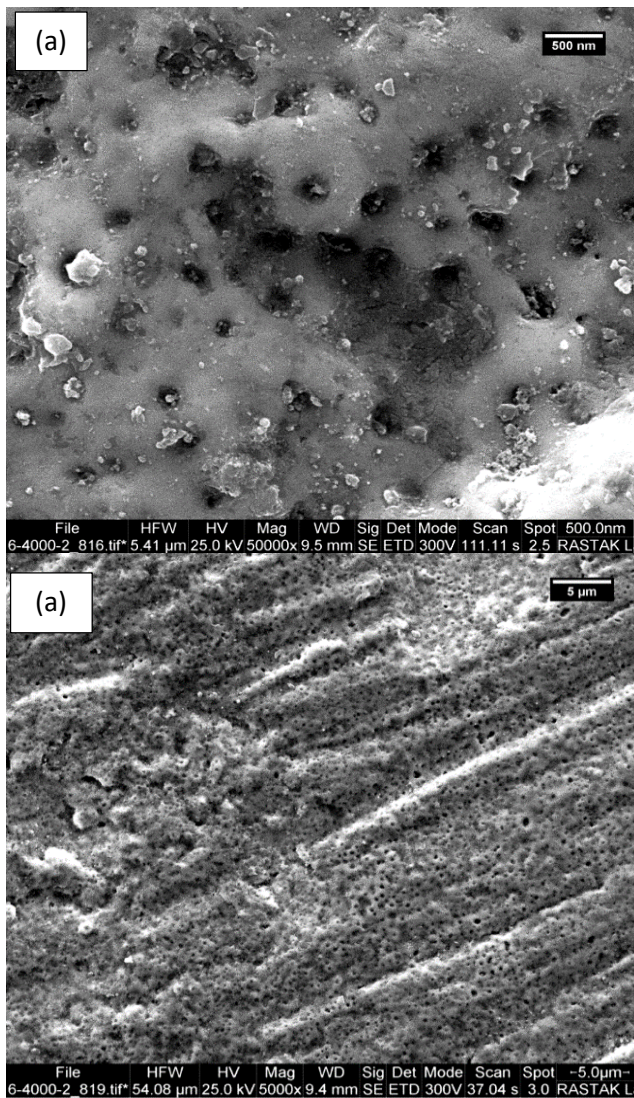


Figure 2. FESEM micrographs of  $\text{TiO}_2$  coating by PEO process (a) at 5min, and (b) 10min.

The surface microstructure of the samples coated in electrolytes containing  $\text{ZrO}_2$  is captured in FESEM images. The surface of the PEO film was discovered to have a low porosity microstructure, and these distributed particles are thought to be a result of the  $\text{ZrO}_2$  that was introduced to the electrolyte in Fig.3 (a). In addition to creating the reaction channels between electrolytes and substrates, the PEO film's restricted porosity also gave rise to the channels

through which molten oxides were expelled throughout the PEO process. The surface morphology seemed more homogenous. The  $ZrO_2$  is precipitation present as aggregate on the surface by small pores distribution on the surface, which leads to enhanced roughness of coatings. In Fig.3 (b) increasing the time led to increasing concentrations of  $ZrO_2$  coating structure and increasing the size of pores and tunnels.



**Figure 3. FESEM micrographs of  $ZrO_2/TiO_2$  nanocomposite coating by PEO process (a) at 5min, and (b) 10min.**

#### Element composition analysis of the coating

The EDX is a type of X-ray emission used to identify the chemical properties of the samples; on the other hand, each element has its atomic structure and specific values in x-ray spectroscopy<sup>30</sup>. The schematic data of EDS results for PEO  $TiO_2$  coatings with different times containing Ti, O, Al, and Nb ions. EDS analysis showed that increasing time had effects on the content, of oxide as shown in Fig. 4 (a, and b) for A1, and A2 samples coated with different time. The existence of Ti and O<sub>2</sub> elements in the coatings, referred to the formation of  $TiO_2$  layers with different weights of these modification

elements. Incorporation of  $ZrO_2$  nanoparticles precipitation by PEO coatings onto the implant surfaces can affect the concentrations of elements (Zr, O, Al, Nb, and Ti) at different times. The ratio of Zr/O<sub>2</sub> was dependent on time, it was 1.09 for (5min) and 12.78 for (10min) as shown in Fig. 4 (c, and d).

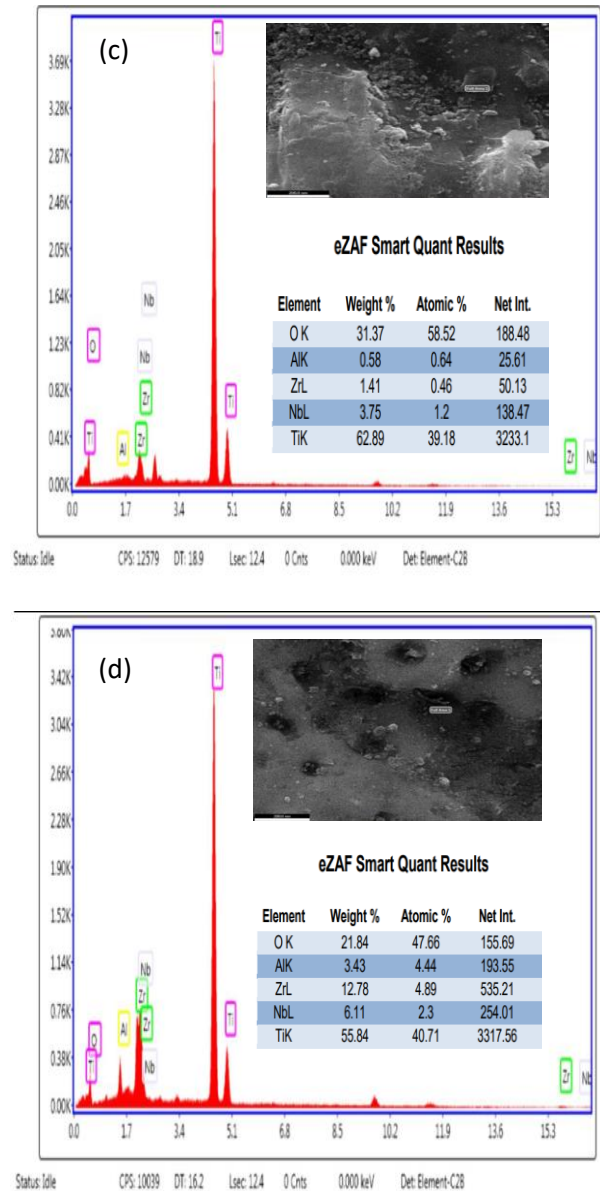
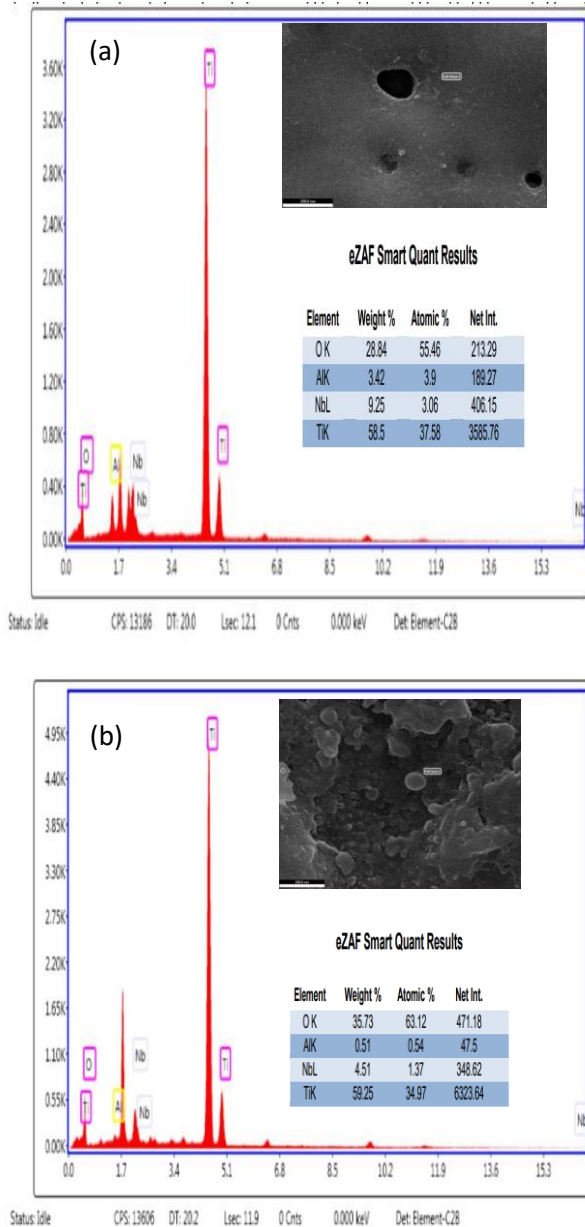


**Figure 4. EDS result of TiO<sub>2</sub>, and ZrO<sub>2</sub>/TiO<sub>2</sub> by PEO Process with different time (a) A1 sample, (b) A2 sample, (c) B1 sample, and (d) B2 sample.**

### Contact Angle Test

Contact angle is a vital measuring tool for assessing a material's surface wettability, which has been discovered to be a key factor in enhancing titanium surfaces' bioactivity. The contact angles tested for TiO<sub>2</sub> by PEO coatings prepared at various deposition times in Hank's solution as shown in Fig. 4. The contact angle of the specimen decreases dramatically after PEO treatment with increase in surface roughness and porosity. The contact angle reached a value equal to (56.74° for the substrate) and decreased with increasing deposition time to (3.1° for sample A1). The PEO treatment resulted in an

uneven coating surface, increased roughness, increased absorbability, and decreased contact angles, all of which jointly influenced the surface energy; and the OH and O<sub>2</sub> oxygen-containing groups generated on the coating surface successfully inhibited surface oxidation. Consequently, the PEO treated material had improved wettability because a high number of micro/nano-pores developed on the oxidation coating surface, leading its specific surface area to rise, which helped water retention<sup>31</sup>. The contact angle on the surface of ZrO<sub>2</sub>/TiO<sub>2</sub> prepared with different oxidation times equal to (11.667° in Hank's solution) for sample B1 increase by increase time to (21.694°) for sample B2 because the wettability is mainly determined by surface

roughness and presence of nanoparticles of ZrO<sub>2</sub> in the electrolytic solution decreased the micro-pores. The implant and human cells may connect more quickly when treated with PEO<sup>32</sup>. Due to the rapid surface protein absorption upon blood-implant contact, high wettability may have a major impact on biocompatibility during implantation. Additional antibacterial effects might be produced by the hydrophobic surface's antifouling characteristics. On the other side, it could reduce the surface-attachment of cells. Extra antimicrobial action from the surface is possible. Conversely, it could make cells less attached to the surface<sup>33,34</sup>.

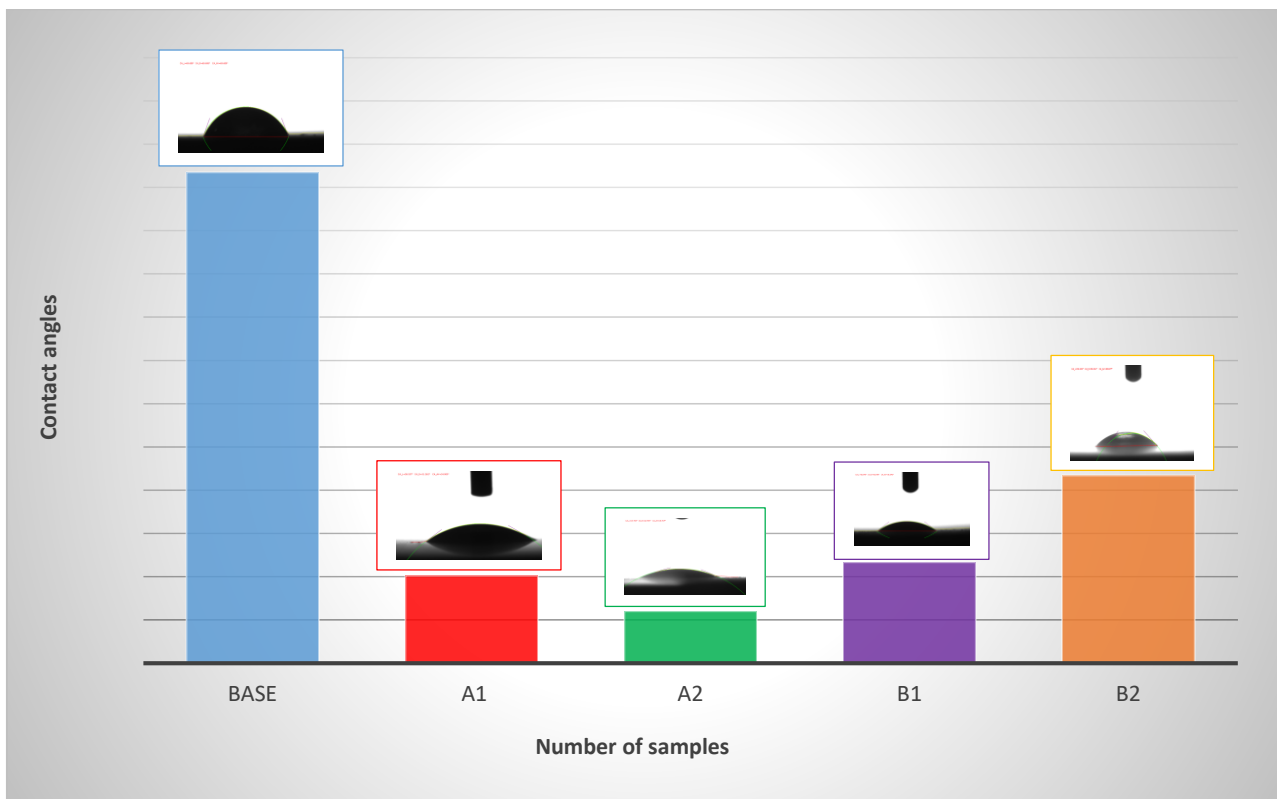


**Figure 5. Results of contact angle of base, TiO<sub>2</sub>, and ZrO<sub>2</sub>/TiO<sub>2</sub> coating by MAO process at 400V with different times in Hanks's solution.**

#### Corrosion Resistance test of MAO coatings

Potentiodynamic and cyclic polarization experiments are used to investigate the corrosion behavior of coatings. The sample is initially submerged in Hank's solution, and after this, time the open circuit potential (OCP), which indicates that a steady state potential has been reached, has been recorded. Different periods and coatings have been examined in relation to corrosion behavior.

#### Open Circuit Potential (OCP)- Time Measurements

It is possible to use the open circuit potential (OCP) variations over time as a gauge of corrosion behavior since they are connected to the sorts of reactions that take place at the electrode surface when it comes into contact with a certain medium (passivation, dissolution, or immunity). In Fig. 6, depicts the Ti6Al7Nb alloy's PEO changes over time in Hank's

solution at  $37^{\circ}\text{C} \pm 1$  along with a comparison to an uncoated alloy. The creation of an oxide coating, which passivates the metallic surface, is said to be the cause of this transformation, according to them. A  $\text{ZrO}_2/\text{TiO}_2$  nanocomposite ceramic coating by the PEO method with varied times in Hank's solution, on the other hand, showed highly stable potentials during the test in the OCP profiles for PEO-treated samples. The PEO sample's OCP grew with time until it stabilized at a stationary value that was more positive for sample B2, but the non-coated sample's scan displayed stable values of nobler potential that were higher than those of the non-coated sample. The variable susceptibility to deterioration of the changed surface may be explained by a number of surface oxide layer factors, including composition, phases, and structural flaws like porosity and cracking.

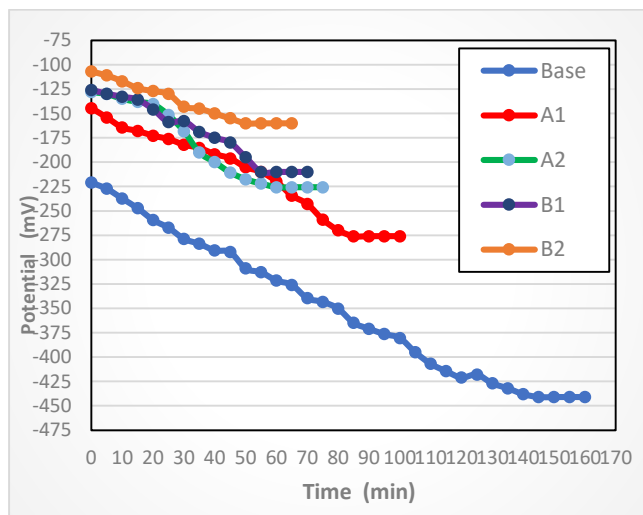


**Figure 6. OCP-time of  $\text{TiO}_2$ , and  $\text{ZrO}_2/\text{TiO}_2$  coating by PEO process in Hank's solution.**

### Potentiodynamic Polarization

The samples for the Ti-6Al-7Nb alloy base,  $\text{TiO}_2$ , and  $\text{ZrO}_2/\text{TiO}_2$  coating by the PEO method that were potentiodynamically polarized over time in Hank's solution at  $37^{\circ}\text{C}$  are shown in Fig. 7. Using Tafel extrapolation, the corrosion potentials ( $E_{\text{corr.}}$ ) and current densities ( $i_{\text{corr.}}$ ) are calculated from the potentiodynamic curves and are shown in Table 3. Additionally, this Table included corrosion rates ( $C_R$ ). Due to the presence of metal ions dissolving on its surface, the uncoated substrate exhibits lower corrosion resistance and a greater corrosion current density ( $i_{\text{corr.}} = 6.8284 \text{ A/cm}^2$ ). The corrosion current density and rate of all coated samples have decreased after coating with  $\text{TiO}_2$ , which indicates that the  $\text{TiO}_2$  coating has created a protective layer on the substrate

surface that has slowed the rate of corrosion. Corrosion resistance is improved when coating at (5min) since it results in the lowest corrosion current ( $i_{\text{corr.}} = 4.619 \text{ A/cm}^2$ ) for sample A1 and boosts the specimens' corrosion potential. Additionally, the film's surface composition has an impact on how corrosive is the material. Reduced corrosion current density and corrosion rate were attained for sample A2 at ( $i_{\text{corr.}} = 3.377 \text{ A/cm}^2$ ), ( $C_R = 4.173 \times 10^{-3} \text{ mpy}$ ), for materials with denser and thicker oxide coatings (10min). The investigation of the corrosive behavior of porous metallic materials in the present work clearly demonstrates the oxygen/air trapped in the deepest holes of porous metallic materials and the challenges of electrolyte penetration into these pores, which may result in various passive states on the native oxide surface. However, the rate at which very porous materials erode is influenced by several factors, not only surface area. It has been asserted that the increased corrosion density with increased porosity level is caused by the larger surface area in contact with the electrolyte, even though Ti is well known for its excellent resistance to localized corrosion and the localized breakdown of its passive coating occurs at comparatively higher potentials. However, less intense corrosion rates may be caused by cracks or restrictions on the entry of species into the connected pores. Excellent passivation qualities are still mentioned in the literature for porous Ti structures, despite the possibility that these challenges would accelerate the kinetics of corrosion. On the other side, it has also been noted that increased porosity reduces corrosion susceptibility (smaller negative  $E_{\text{corr.}}$  values), since interconnected holes encourage the free passage of ionic species, whereas isolated pores confine the electrolyte and deplete the oxygen supply, resulting in a thinner oxide coating. Aside from species free movement, air entrapment, and electrolyte penetration<sup>35</sup>. One of the two goals of surface modification of medical alloys is to prevent corrosion, which requires a surface free of pores to reduce the attachment of active ions to the base metal, and the second goal is to create a rough and porous surface to improve the bonding between tissue and implants<sup>36</sup>. The efficacy of the  $\text{ZrO}_2/\text{TiO}_2$  nanocomposite ceramic coating by the PEO process with different times in the corrosion resistance, has been investigated in Hank's solution. The maximum corrosion resistance for sample B1 is achieved after coating at (5min), which results in the lowest corrosion current density ( $i_{\text{corr.}} = 1.673 \text{ A/cm}^2$ ). The

surface shape and phases generated in the composite film have a significant impact on the  $ZrO_2/TiO_2$  coating's ability to improve corrosion resistance. By preventing the assault from ( $Cl^-$ ) ions in Hank's solution, a denser, thicker coating with fine porosity is more beneficial for enhancing corrosion resistance<sup>37</sup>. With increased time corrosion resisters increased by decreased corrosion current density ( $i_{corr.}$ ) from ( $0.662 \mu A/cm^2$ ) and corrosion rate ( $C_R$ ) equal ( $0.8 \times 10^{-3}$ ) for sample B2 by increased concentration of  $ZrO_2$  in the electrolytic. Moreover, the presence of porosity in the microstructure allows the penetration of the corrosive fluid into the substrate and corrodes it. The corrosion potential ( $E_{corr.}$ ) for the coated samples raises toward values that are more positive when PEO. There are brittle fractures that may have an impact on the formation of passive regions, but this did not stop the improvement in  $I_{corr.}$ . Factors that influence coating corrosion characteristics include crystallinity, purity, brittle fractures, porosity, and ion penetration into the coating<sup>38</sup>.

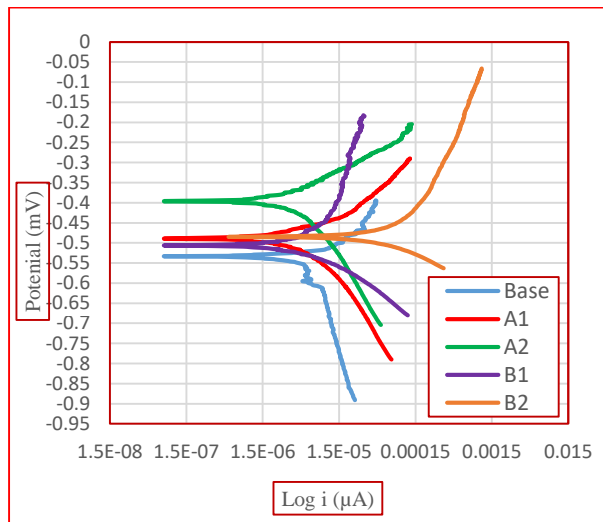


**Figure 7. Potentiodynamic polarization curves of  $TiO_2$ ,  $ZrO_2/TiO_2$  coated by PEO process and base at different time and applied voltages 400V in Hank's solution.**

**Table 4. Electrochemical parameters of base,  $TiO_2$  and  $ZrO_2/TiO_2$  nanocomposite coated by PEO at different time in hank's solution.**

Sample Code	$E_{corr.}$ (mV)	$i_{corr.}$ ( $\mu A/cm^2$ )	$C_R^* 10^{-3}$ (mpy)	Improvement percentage (%)
Base	-579	6.828	8.777	/
A1	-506	4.619	5.7	32.4
A2	-396	3.377	4.173	50.5
B1	-485	1.673	1.712	80
B2	-489	0.662	0.8	90.5

### Cycle Polarization Test

The increased ion release rates brought on by various types of localized corrosion may eventually cause implant loosening due to a chain of unfavorable biological reactions. By using cyclic polarization, corrosion susceptibility to several types of corrosion is assessed. The characteristics discovered by analyzing the current-voltage curve can be connected to the localized corrosion mechanism. The reading typically begins at open circuit potential and scans upward until breakdown is reached. Afterwards, the direction of the scan is reversed after a particular amount of localized corrosion has been established and the passive film has been harmed<sup>39</sup>. It is possible for a stable pit ( $E_p$ ) to form at a certain potential, which is known as the breakdown potential ( $E_b$ ). As a result, the  $E_p$  makes reference to the potential that the trenches grew from. If the  $E_p$  is high, the material has strong resistance to pitting corrosion. The resistance of the sample is shown by the difference ( $\Delta E$ ) between  $E_p$  and  $E_{prot}$ ; the stronger the corrosion resistance, the lower the  $E$  value. (Fig. 8) shows the polarization curves obtained for uncoated Ti6Al7Nb and  $TiO_2$ ,  $ZrO_2/TiO_2$  coating by PEO process with different time in Hank's solution. There were observable discrepancies in the curves obtained for each sample. The Ti-6Al-7Nb alloy has the lowest  $E_p$  and  $E_{prot}$  values when compared to the  $TiO_2$  specimens that have undergone the PEO process' susceptibility to pitting corrosion. The cyclic polarization curves for  $TiO_2$  at various points in time. As shown in Table 5, the hysteresis loop's size is significantly reduced, which makes the corrosion mechanism working on the substrate surface less active. But for sample A2, the PEO process settings were adjusted to ( $E_p = -180mV$ ). Considering the randomness of the PEO process itself, the porosity of the oxide coatings, and the local in homogeneity of the samples, the results obtained are relatively constant, and the variances dis the values are minimal. The sample with the  $ZrO_2/TiO_2$  nanocomposite coating has the maximum pitting and protection potential ( $E_p = -204mV$ ) for sample B1 with an open hysteresis loop, where this polarization behavior tends to be resistive to the localized corrosion. Additionally, sample B2 has the lowest value of ( $E_p = -316 mV$ ), meaning that it will have greater resistance to pitting corrosion as voltage and time increase. This indicates that the pit start, and propagation have been appropriately hampered by this sample. Longer deposition times or higher current densities during the PEO process are

predicted to result in greater corrosion resistance (influenced by film characteristics). With more voltage and time, they exhibit remarkable resistance to pitting corrosion. This is related to the fact that the film features rely on tiny alterations to the PEO process parameters and that, in certain cases, uneven surfaces are formed as a result of the film's gradual degradation. A composite layer coating is produced as a result of the PEO process's cyclical nature, which causes the initially generated anodic oxide to be broken down and then later recreated, albeit at a fixed current density throughout the process time. This leads to an inconsistency in the measured corrosion parameters. The minimal standard in the results, however, highlights how similar the corrosion properties are between samples treated with the same PEO procedure parameters and timeframes. Consequently, the deposition of TiO<sub>2</sub>, and ZrO<sub>2</sub>/TiO<sub>2</sub> on Ti-6Al-7Nb alloy has an excellent chemical stability, bioactivity, and mechanical integrity. As a result, the osseointegration characteristics could be

enhanced and employed as a biofilm for applications involving hard tissue implants.

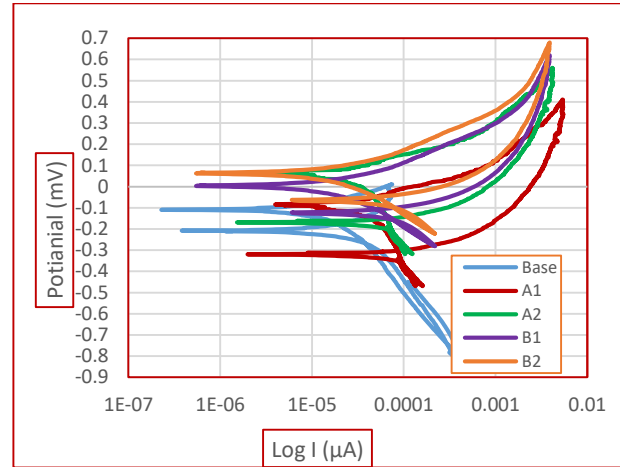


**Figure 8. Cycle polarization curves of TiO<sub>2</sub>, and ZrO<sub>2</sub>/TiO<sub>2</sub> coated by PEO process and base at different time and applied voltages 400V in Hank's solution.**

**Table 5. Values of electrochemical parameters of of base, TiO<sub>2</sub> and ZrO<sub>2</sub>/TiO<sub>2</sub> nanocomposite coated by PEO at different time in hank's solution from cyclic polarization.**

Sample Code	$i_{corr.}$ ( $\mu A/cm^2$ )	$E_p.$ (mV)	$E_{prot}$ (mV)	$\Delta E = (E_p - E_{prot})$ (mV)	$C_R * 10^{-3}$ (mpy)	Improvement percentage (%)
Base	7.164	-780	-630	-150	8.852	/
A1	3.572	-270	-100	-170	4.413	50
A2	2.004	-180	80	-260	2.476	72
B1	1.484	-204	-30	-274	1.833	79.3
B2	0.84	-316	50	-366	1.04	88.25

### Ion release test

An Element of Ti-6Al-7Nb alloy was measured for coated and uncoated samples by using atomic absorption spectrometry in Hank's solution at 37°C±1, PH 7.4 for 21 day. The Titanium ion release concentration shows in (Table 6) of the uncoated sample is (0.0301ppm). The lowest corresponding numbers of coated TiO<sub>2</sub> (0.0183ppm) for sample A1 and equal (0.0074ppm) for sample A2 and (0.0066ppm) for ZrO<sub>2</sub>/TiO<sub>2</sub> coating for sample B1 reduced to (0.0017ppm) for sample B2. This means an improvement (39.2%, 75.4%, 78%, and 94.35%). Aluminum and Niobium ions release concentrations in Hank's solution are shown in this table for the uncoated sample is (0.0172ppm). The lowest corresponding numbers of coated TiO<sub>2</sub> (0.0043 and 0.0030) (ppm) and ZrO<sub>2</sub>/TiO<sub>2</sub> equal (0.0019 and 0.0012) (ppm) concentrations of Al and Nb ions respectively. This means that improvements in Al ion

were (75%, 86.6%, 88.95% and 96%) and Nb ion (80.6%, 84.5%, 93%, and 98.125%).

**Table 6. The Amount of Ti, Al, and Nb ions Concentration in Hank's solution at 37°C.**

Sample Code	Ti	Al	Nb
Uncoated	0.0301	0.0172	0.0155
A1	0.0183	0.0043	0.0030
A2	0.0074	0.0023	0.0024
B1	0.0066	0.0019	0.0012
B2	0.0017	0.0007	0.0004

### Antibacterial Study

The antibacterial effect of the uncoated Ti-6Al-7Nb alloy and coating TiO<sub>2</sub> and nanocomposite ceramics coating layer ZrO<sub>2</sub>/TiO<sub>2</sub> by PEO process. Suspensions were investigated against E. coli culture as shown in (Fig. 9a, b, c, d, and f). The bacterial inhibition zone is indicated by the creation of a clear region surrounding the disc. After a 24-hour

incubation period, it was observed that the coating sample cases had a strong antibacterial activity against *E. coli*. but the uncoated alloy sample has a small inhibition zone as compared with the other coating samples. This is because anatase  $\text{TiO}_2$  is naturally antibacterial, and as a result, the composite particles have a potent antibacterial impact<sup>40</sup>. Therefore, the  $\text{ZrO}_2$  coatings'  $\text{TiO}_2$  nanoparticles were successful in preventing bacterial development that would enhance the antibacterial activity by restricting bacterial adherence to the surface. The thickness of the protective layer also increased with increased deposition time.

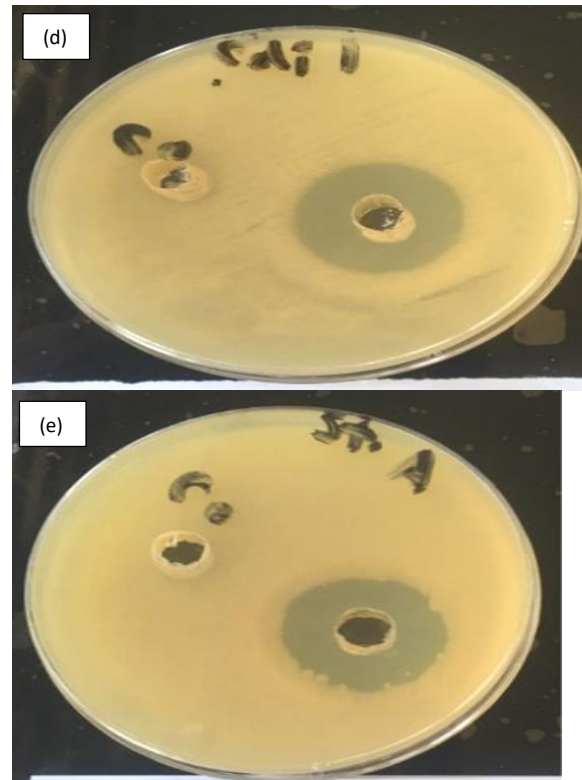
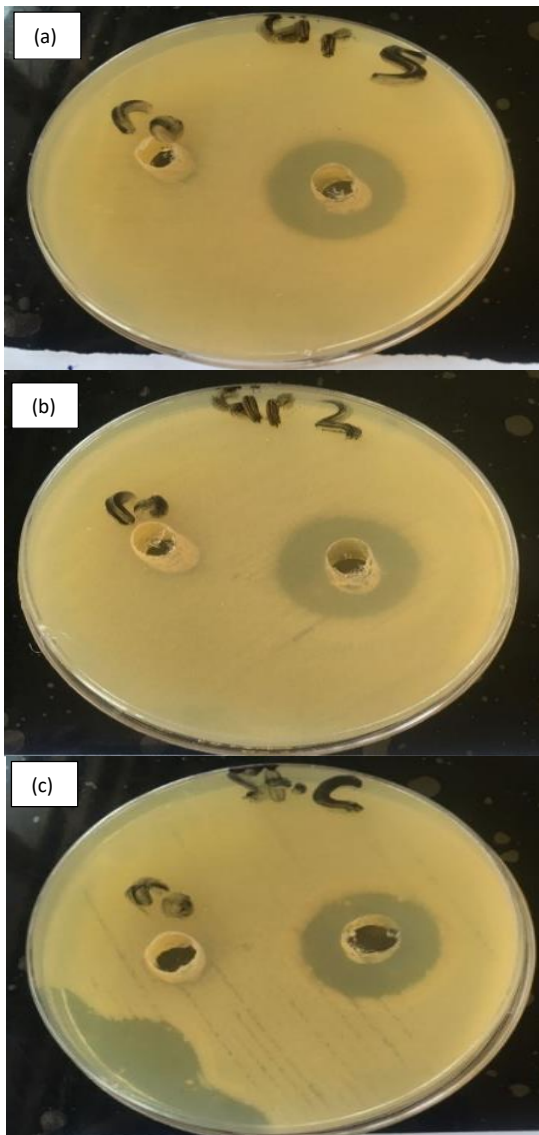


**Figure 9.** Visual representations of *E. coli*'s antibacterial performance are shown in (a) base, (b) A1, (c) A2, (d) B1, and (e) B2.

## Conclusion

Write the in the present work,  $\text{TiO}_2$  and a nanocomposite coating of  $\text{ZrO}_2/\text{TiO}_2$  have been

effectively deposited on the surface of Ti-6Al-7Nb alloy for biomedical applications. It has been found

that the TiO<sub>2</sub> layer developed on the Ti-6Al-7Nb alloy base material using the PEO technique under the prescribed conditions exhibits circular micropores in rough and volcanic structures as a result of ongoing micro discharges happening during the process. The rutile and anatase TiO<sub>2</sub> phases on the material's surface are identified using the XRD analysis. The substrate's surface roughness significantly affects how well the coating adheres to the substrate. The topography on the AFM is uniform and dense. When coating using the optimal conditions for sample B2 at that time, the morphology of composite coatings was uniform and devoid of cracks (400V-10min). The porosity analysis showed that the coating porosity increases with increasing deposition time. EDS results showed that the ratio of Zr/O<sub>2</sub> increased with time at coating ZrO<sub>2</sub>/TiO<sub>2</sub>. The apparent contact angle somewhat reduces following treatment at various times. The surface morphology and composition of the PEO coatings may be the cause of the PEO coatings' considerable shift in apparent contact angle. Due to its smaller pores, the wettability of the PEO coating created at lower roughness may be underestimated. However, due to no gas being trapped and a coarser liquid/solid interface, the wettability of the PEO coating created at higher roughness may be

overestimated. The best result for sample A1 at TiO<sub>2</sub> coating equal ( $i_{corr}=4.619A/cm^2$ ) compared to the uncoated sample was obtained using potentiodynamic polarization of the Ti-6Al-7Nb base material, TiO<sub>2</sub>, and ZrO<sub>2</sub>/TiO<sub>2</sub> nanocomposite coating on Ti-6Al-7Nb alloys at different times in Hank's solution. The nanocomposite coating ZrO<sub>2</sub>/TiO<sub>2</sub> has the lowest corrosion current density value ( $i_{corr.} = 0.856\mu A/cm^2$ ) and highest corrosion resistance equal ( $1.673\mu A/cm^2$ ) for sample B1, and ( $0.662\mu A/cm^2$ ) for sample B2. In addition, the cyclic polarization results state improvement in the pitting corrosion resistance when immersed in the Hank's solution. The ions release concentration (Ti, Al, and Nb) in Hank's solution significantly decreased for the coated samples compared with uncoated sample, as the concentration of ions is lower after being placed for 21 days. This enhancement in reducing titanium, aluminum, and Niobium ions release is more likely due to ZrO<sub>2</sub>/TiO<sub>2</sub> layer provide an adherent and very protective layer. The results of antibacterial analysis have confirmed that the ZrO<sub>2</sub>/TiO<sub>2</sub> nanocomposite coatings reveal a good antibacterial activity against gram negative E.coli which makes this coating safe and can be used for bone implant applications.

### Acknowledgment

The Authors are grateful for the University of Babylon for their help. Special thanks for College of

Materials Engineering/ Metallurgical Engineering department

### Authors' Declaration

- Conflicts of Interest: None.
- We hereby confirm that all the Figures and Tables in the manuscript are ours. Furthermore, any Figures and images, that are not ours, have been included with the necessary permission for re-publication, which is attached to the manuscript.

- Ethical Clearance: The project was approved by the local ethical committee at University of Babylon.
- Ethics statement:  
No animal studies are present in the manuscript.  
No human studies are present in the manuscript.  
No potentially identified images or data are present in the manuscript.

### Authors' Contribution Statement

This work was carried out in collaboration between all authors. From the beginning of the work of preparing samples and conducting the coating

process and tests. All authors read and approved the final manuscript.

### References

1. Kaur M, Singh K. Review on titanium and titanium-based alloys as biomaterials for orthopaedic applications. *Mater Sci Eng C Mater Biol Appl*. 2019; 102: 844-862. <https://doi.org/10.1016/j.msec.2019.04.064>.
2. Dos Santos A G. The Importance of Metallic Materials as Biomaterials. *Adv Tissue Eng Regen Med*. 2017; 3(1): 300-302. <https://doi.org/10.15406/atroa.2017.03.00054>.
3. Mozetič M. Surface Modification to Improve Properties of Materials. *Materials*. 2019; 12(3): 441. <https://doi.org/10.3390/ma12030441>.
4. Kaur S, Ghadirinejad K, Oskouei R H. An overview on the tribological performance of titanium alloys with surface modifications for biomedical applications. *Lubricants*. 2019; 7(8). <https://doi.org/10.3390/lubricants7080065>.
5. Bahl S, Suwas S, Chatterjee K. Comprehensive review on alloy design, processing, and performance of  $\beta$  Titanium alloys as biomedical materials. *Int Mater Rev*. 2021; 66(2): 114-139. <https://doi.org/10.1080/09506608.2020.1735829>.
6. Campoccia D, Montanaro L, Arciola C.R. A review of the biomaterials technologies for infection-resistant surfaces. *Biomater*. 2013; 34(34): 8533-8554. <https://doi.org/10.1016/j.biomaterials.2013.07.089>.
7. Thair L, Mudali U K, Bhuvaneshwaran N, Nair K G M, Asokamani R, Raj B. Nitrogen ion implantation and in vitro corrosion behavior of as-cast Ti-6Al-7Nb alloy. *Corros Sci*. 2002; 44(11): 2439-2457. [https://doi.org/10.1016/S0010-938X\(02\)00034-3](https://doi.org/10.1016/S0010-938X(02)00034-3).
8. Wu G, Li P, Feng H, Zhang X, Chu P.K. Engineering and functionalization of biomaterials via surface modification. *J Mater Chem B*. 2015; 3(10): 2024-2042. <https://doi.org/10.1039/C4TB01934B>.
9. Sidambe AT. Biocompatibility of advanced manufactured titanium implants-A review. *Materials*. 2014; 7(12): 8168-8188. <https://doi.org/10.3390/ma7128168>.
10. Kawano M, Takeda Y, Ogasawara K. Pathological Analysis of Metal Allergy to Metallic Materials. *Advances in Metallic Biomaterials 2015*: 305-321. [https://doi.org/10.1007/978-3-662-46836-4\\_13](https://doi.org/10.1007/978-3-662-46836-4_13).
11. Dos Santos G.A. The Importance of Metallic Materials as Biomaterials. *Adv Tissue Eng Regen Med*. 2017; 3(1): 300-302. <https://doi.org/10.15406/atroa.2017.03.00054>.
12. Shaikh S, Kedia S, Singh D, Subramanian M, Sinha S. Surface texturing of Ti6Al4V alloy using femtosecond laser for superior antibacterial performance. *J Laser Appl*. 2019; 31(2). <https://doi.org/10.2351/1.5081106>.
13. Leng Y X, Chen J Y, Yang P, Sun H, Huang N. Structure and properties of passivating titanium oxide films fabricated by DC plasma oxidation. *Surf Coatings Technol*. 2003; 166(2-3): 176-182. [https://doi.org/10.1016/S0257-8972\(02\)00780-6](https://doi.org/10.1016/S0257-8972(02)00780-6).
14. Chikarakara E. In vitro fibroblast and pre-osteoblastic cellular responses on laser surface modified Ti-6Al-4V. *Biomed Mater*. 2015; 10(1). <https://doi.org/10.1088/1748-6041/10/1/015007>.
15. Kurup A, Dhatrak P, Khasnis N. Surface modification techniques of titanium and titanium alloys for biomedical dental applications: A review. *Mater Today Proc*. 2020; 39: 84-90.
16. Bosco R, Van Den Beucken J V, Leeuwenburgh S, Jansen J. Surface engineering for bone implants: A trend from passive to active surfaces. *Coatings*. 2012; 2(3): 95-119. <https://doi.org/10.3390/coatings2030095>.
17. Kulkarni M, Mazare A, Schmuki P, Igljč A. Titanium nanostructures for biomedical applications. *Nanotechnology*. 2015. 26(6). <https://doi.org/10.1088/0957-4484/26/6/062002>.
18. Zhang L C, Chen L Y. A Review on Biomedical Titanium Alloys: Recent Progress and Prospect. *Adv Eng Mater*. 2019; 21(4): 1-29. <https://doi.org/10.1002/adem.201801215>.
19. Liu Xuanyong, Chu Paul K, Chuanxian D. Surface modification of titanium, titanium alloys, and related materials for biomedical applications. *Mater Sci Eng R*. 2004; 47(3-4): 49-121. <https://doi.org/10.1016/j.mser.2004.11.001>.
20. Dorozhkin S V. Calcium orthophosphate deposits: Preparation, properties and biomedical applications. *Mater Sci Eng C*. 2015; 55: 272-326. <https://doi.org/10.1016/j.msec.2015.05.033>.
21. Mohammed M T, Khan Z A, Siddiquee A N. Surface Modifications of Titanium Materials for developing Corrosion Behavior in Human Body Environment: A Review. *Procedia Mater Sci*. 2014; 6(Icmpc): 1610-1618. <https://doi.org/10.1016/j.mspro.2014.07.144>.
22. Liu X, Chu P, Ding C. Surface Modification of Titanium, Titanium alloys, and related materials for biomedical applications. *Mater Sci Eng R*. 2004; 47(3-4): 49-121. <https://doi.org/10.1016/j.mser.2004.11.001>.
23. Zaynab N, Rahseed A. Water Temperature Effect on Hardness and Flexural Strength of (PMMA/TiO<sub>2</sub>NPs) for Dental Applications. *Baghdad Sci J*. 2022; 19(4): 922-931. <https://doi.org/10.21123/bsj.2022.19.4.0922>.
24. Prakash C, Singh S, Singh R. Current Trends in Biomaterials and Bio-manufacturing. In Book: *Biomanufacturing*. Chap 1, 2019; p. 1-271. [https://doi.org/10.1007/978-3-030-13951-3\\_1](https://doi.org/10.1007/978-3-030-13951-3_1).
25. Michael A. Enhancing Corrosion Performance of Laser Modified NiTi Shape Memory Alloy: MSc Diss. Of Applied Science in Mechanical Engineering, University of Waterloo, Ontario, Canada. 2014.
26. Santos-Coquillat A, Gonzalez Tenorio R, Mohedano M, Martinez-Campos E, Arrabal R, Matykina E. Tailoring of antibacterial and osteogenic properties of Ti6Al4V by plasma electrolytic oxidation. *Appl Surf*

- Sci. 2018; 454: 157–172.  
<https://doi.org/10.1016/j.apsusc.2018.04.267>.
27. De Viteri V S. Structure, tribocorrosion and biocide characterization of Ca, P and I containing TiO<sub>2</sub> coatings developed by plasma electrolytic oxidation. *Appl Surf Sci.* 2016; 367: 1-10.  
<https://doi.org/10.1016/j.apsusc.2016.01.145>
28. Xu L. Effect of oxidation time on cytocompatibility of ultrafine-grained pure Ti in micro-arc oxidation treatment. *Surf Coatings Technol.* 2018; 342: 12–22.  
<https://doi.org/10.1016/j.surfcoat.2018.02.044>.
29. Campanelli L C, Duarte L T, da Silva P S C P, Bolfarini C. Fatigue behavior of modified surface of Ti-6Al-7Nb and CP-Ti by micro-arc oxidation. *Mater Des.* 2014; 64: 393–399.  
<https://doi.org/10.1016/j.matdes.2014.07.074>.
30. Zainab R, Abbas Ali S, Farqad A, Labeeb A, Suha Mohamed I. An Evaluation of the Activity of Prepared Zinc Nanoparticles with Extracted Alfalfa Plant in the Treatment of Heavy Metals. *Baghdad Sci J.* 2022; 19(6): 1399-1409.  
<https://doi.org/10.21123/bsj.2022.7313>.
31. Cunha A. Multiscale femtosecond laser surface texturing of titanium and titanium alloys for dental and orthopaedic implants To cite this version: PhD theses. Université de Bordeaux. 2015; HAL Id : tel-01215468.
32. Wang C. The influence of alloy elements in Ti–6Al–4V and Ti–35Nb–2Ta–3Zr on the structure, morphology and properties of MAO coatings. *Vacuum.* 2018; 157: 229–236.  
<https://doi.org/10.1016/j.vacuum.2018.08.054>.
33. Alves A C. Effect of bio-functional MAO layers on the electrochemical behaviour of highly porous Ti. *Surf Coatings Technol.* 2020; 386125487.  
<https://doi.org/10.1016/j.surfcoat.2020.125487>.
34. Yang W, Xu D, Guo Q. Influence of electrolyte composition on microstructure and properties of coatings formed on pure Ti substrate by micro arc oxidation. *Surf Coatings Technol.* 2018; 349: 522-528.  
<https://doi.org/10.1016/j.surfcoat.2018.06.024>.
35. Sedelnikova M B. Functionalization of pure titanium MAO coatings by surface modifications for biomedical applications. *Surf Coatings Technol.* 2020; 394: 125812.  
<https://doi.org/10.1016/j.surfcoat.2020.125812>.
36. Lara Rodriguez L, Sundaram P.A. Corrosion behavior of plasma electrolytically oxidized gamma titanium aluminide alloy in simulated body fluid. *Mater Chem. Phys.* 2016; 181: 67–77.  
<https://doi.org/10.1016/j.matchemphys.2016.06.034>.
37. Teng H P, Lin H Y, Huang Y H, Lu F H. Formation of strontium-substituted hydroxyapatite coatings on bulk Ti and TiN-coated substrates by plasma electrolytic oxidation. *Surf Coatings Technol.* 2018; 350: 1112-1119.  
<https://doi.org/10.1016/j.surfcoat.2018.02.017>.
38. Eliaz N. Corrosion of metallic biomaterials: A review. *Materials.* 2019; 12(3).  
<https://doi.org/10.3390/ma12030407>.
39. Metikoš-Huković M, Kwokal A, Piljac J. The influence of niobium and vanadium on passivity of titanium-based implants in physiological solution. *Biomater.* 2003; 24(21): 3765-3775.  
[https://doi.org/10.1016/S0142-9612\(03\)00252-7](https://doi.org/10.1016/S0142-9612(03)00252-7).
40. Khalaf H, Abdulhamied Z, Dawod A. Effect of surface modification of Si wafers on solar cell efficiency ZnO/P-Si thin films prepared by plasma sputtering. *IOP Conference Series: Mater Sci Eng.* 2019; 571(1).  
<https://doi.org/10.1088/1757-899X/571/1/012115>.

## طلاء المركب النانوي لسبيكة Ti-6Al-7Nb بواسطة اكسدة التحلل الكهربائي للبلازما PEO واستخدامها في التطبيقات الطبية

قيس خالد ناجي ، جاسم محمد سلمان ، نوال محمد داوود

قسم المعادن، كلية هندسة المواد ، جامعة بابل ، بابل، العراق.

### الخلاصة

تهدف الدراسة الحالية إلى استخدام سبيكة Ti-6Al-7Nb بدلاً من سبيكة Ti-6Al-4V في التطبيقات الطبية. وبسبب بصلاقتها المنخفضة ومقاومة البلى التي تسبب فقدان الزرع. تم طلاء سطح سبيكة Ti-6Al-7Nb بطبقة مركبة من أكسيد تيتانيوم وأكسيد الزركونيا النانوية بواسطة عملية الأكسدة بالتحليل الكهربائي للبلازما (PEO). أظهرت نتائج الاختبارات إمكانية ترسيب طلاء السيراميك على سطح سبيكة Ti-6Al-7Nb باستخدام فترات زمنية مختلفة. طبقة السيراميك من أكسيد التيتانيوم (TiO<sub>2</sub>) والتي تتكون أثناء الطلاء المسامي، والتوزيع المتجانس، ومقاومة التآكل العالية وقابلية البلى. تم الحصول على طبقة نانوية سيراميك مركبة من ZrO<sub>2</sub> مع TiO<sub>2</sub> ولوحظ مع زيادة الوقت يزداد من سمك طبقة الطلاء وتركيز ZrO<sub>2</sub> وانخفاض المسامية مقارنة بطبقة TiO<sub>2</sub> بنسبة التحسين (90.5%) مع قدرة قوية على تكوين حاجز لمنع هجوم التآكل الموضعي من قبل الأيونات العدوانية التي ظهرت في محلول هانك أثناء اختبار التآكل.

**الكلمات المفتاحية:** مقاومة التآكل، تطبيقات الطبية، الأكسدة بالتحليل الكهربائي للبلازما (PMA)، المسامية، أكسيد التيتانيوم (TiO<sub>2</sub>).